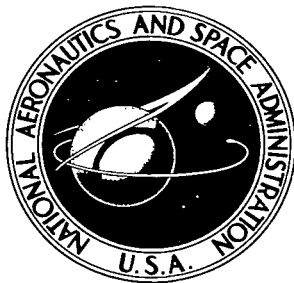


NASA TECHNICAL NOTE



NASA TN D-4058

c.1

LOAN COPY SENT
AT THE REQUEST OF
KIRTLAND AFB, TX



0130763

NASA TN D-4058

ION CYCLOTRON WAVE GENERATION IN UNIFORM AND NONUNIFORM PLASMA INCLUDING ELECTRON INERTIA EFFECTS

by Donald R. Sigman and John J. Reinmann

*Lewis Research Center
Cleveland, Ohio*



NATIONAL AERONAUTICS AND SPACE ADMINISTRATION • WASHINGTON, D. C. 20546 JULY 1967



ION CYCLOTRON WAVE GENERATION IN UNIFORM AND NONUNIFORM
PLASMA INCLUDING ELECTRON INERTIA EFFECTS

By Donald R. Sigman and John J. Reinmann

Lewis Research Center
Cleveland, Ohio

NATIONAL AERONAUTICS AND SPACE ADMINISTRATION

For sale by the Clearinghouse for Federal Scientific and Technical Information
Springfield, Virginia 22151 - CFSTI price \$3.00



CONTENTS

	Page
SUMMARY	1
INTRODUCTION	1
THEORY	2
Equations of Motion and Maxwell's Equations	3
Boundary Conditions	6
Vacuum Solutions	7
Homogeneous Plasma (Solid or Annular)	8
Power Transfer to Homogeneous Plasma	11
R'_n for Homogeneous Plasma	14
Inhomogeneous Plasma	15
RESULTS AND DISCUSSION	17
Current-Sheet Representation	18
Coil Radius	19
Frequency	20
Solid Cylinder of Constant-Density Plasma	21
Plasma density	22
Current-sheet wavelength	22
Plasma radius	23
Dispersion relation for finite electron mass	23
Variable Density and Annular Plasmas	27
Different Plasma Modes	30
Effect of Temperature and Collisions	31
Wave Reflections	32
CONCLUSIONS	33
APPENDIXES	
A - SYMBOLS	35
B - FUNCTIONS $\Gamma(k)$ AND MATRIX M	39
C - SOLVING FOR NATURAL MODES	42
REFERENCES	44

ION CYCLOTRON WAVE GENERATION IN UNIFORM AND NONUNIFORM PLASMA INCLUDING ELECTRON INERTIA EFFECTS

by Donald R. Sigman and John J. Reinmann

Lewis Research Center

SUMMARY

Theoretical calculations were made for radiofrequency power transfer to ion cyclotron waves from a Stix coil. The analysis includes electron inertia terms and is applied to a cylindrical column of cold, collisionless atomic-hydrogen plasma with and without radial density variations. The results showed both an optimum coil wavelength and an optimum density for efficient power transfer. For typical plasmas, the optimum density is between 1×10^{12} and 5×10^{12} per cubic centimeter. Without a radial density gradient, the inclusion of the electron inertia terms reduced the predicted power transfer. Several radial density distributions were considered. Power transfer to inhomogeneous plasmas is maximum when the volume average density is near the optimum density computed for homogeneous plasmas. Curves of power absorption as a function of magnetic field for inhomogeneous plasmas were similar to those for constant density. Under some conditions, radiofrequency power is coupled predominantly to a single plasma mode of oscillation; under other conditions, the power may be distributed among several modes. Thus, measurements of plasma wave properties may prove difficult to interpret.

INTRODUCTION

The thermalization of ion cyclotron waves in a plasma column offers a promising technique for heating plasma ions to extremely high temperatures. Stix (ref. 1) devised a generating structure (radiofrequency coil) to couple radiofrequency power to ion-cyclotron waves efficiently and has also made a careful theoretical analysis of the power-coupling process. In his theory, Stix assumed a cold, collisionless magnetoplasma and neglected electron inertia terms in the equations of motion. In reference 2, Stix's theory was employed to determine the effect of various plasma and radiofrequency coil parameters on the power transfer to ion cyclotron waves in a homogeneous, atomic-hydrogen

plasma. In the present report, the parametric analysis is repeated, but electron mass is not assumed to be zero. Furthermore, both homogeneous and radially inhomogeneous plasmas are considered. The results of this report were first presented at the 1966 Summer Meeting of the American Physical Society, Minneapolis, Minnesota.

As in references 1 and 2, the radiofrequency coil is represented by an azimuthal current sheet of finite length wrapped around an infinitely long plasma column that is placed in a vacuum. The plasma is immersed in a steady and uniform magnetic field parallel to the axis of the column.

In the region underneath the finite-length current sheet, power is transferred to the ion cyclotron wave. This wave propagates unattenuated out both ends of the cylindrical current sheet and down the plasma column. Since the plasma model is cold and collisionless, all energy from the current sheet is converted to electromagnetic energy in the wave.

The theoretical analysis proceeds as follows: Maxwell's equations are employed with the equations of motion for the plasma ions and electrons in order to derive the fourth-order partial differential equations for the electric and magnetic fields in the plasma. Then, expressions are obtained for the fields under infinitely long current sheets with wave number k . Following a Fourier integral technique used by Stix (ref. 1), one uses the fields derived for infinitely long current sheets to obtain the fields produced by a finite-length current sheet. For the homogeneous plasma, a dispersion relation is derived.

The equations derived herein were used to make digital computer calculations to determine the effects of coil wavelength, overall coil length and radius, magnetic field, plasma density, and plasma radius on the power transfer to ion cyclotron waves in a homogeneous plasma. In addition, sufficient calculations were made for inhomogeneous plasmas and for an annular cylinder of plasma of uniform density to determine the major effect of radial density variations on power transfer.

The assumption of zero electron mass simplifies the problem considerably. Early attempts by the authors of this report to extend the analysis of reference 2 to inhomogeneous plasmas resulted in the prediction of unrealistically low power-transfer efficiencies for slight departures from uniformity. Furthermore, the findings of reference 2 yield the unrealistic result that maximum power transfer monotonically increased as the density decreased. The inclusion of electron mass in the analysis removed both these difficulties.

THEORY

To derive equations for radiofrequency power transfer to a plasma, a geometric configuration similar to that used by Stix (ref. 1) is assumed. The elements of the config-

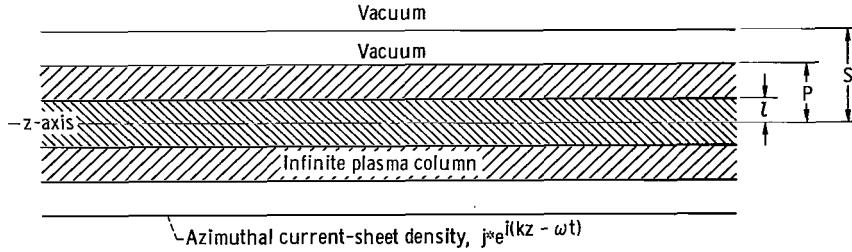


Figure 1. - Plasma column and current sheet.

uration are shown in figure 1. A cylinder (solid or annular) of cold plasma, infinitely long, is assumed to be surrounded by vacuum. A uniform, static magnetic field B_0 (maintained by external coils) is parallel to the z-axis of the cylinder. The outer radius of the plasma is p , and the inner radius is ℓ . For a solid cylinder of plasma, the inner radius ℓ is zero. At the radius $r = s$ (where $s > p$), there is an azimuthal current sheet of density $j_0 e^{i(k_0 z - \omega t)}$, where k_0 is the current-sheet wave number for the z-direction. Because the current sheet for the case of interest is of finite length, it is necessary to apply a Fourier integral analysis (ref. 1) to express the finite-length sheet as an integral over k of a continuous spectrum of azimuthal current-sheet components, each of which can be considered to be of infinite length. In this approach, the equations are formulated for an infinite-length current sheet and then are combined in the manner indicated by the Fourier integral analysis to obtain the results for the finite sheet.

Equations of Motion and Maxwell's Equations

For an infinitely long current sheet, the time-varying electric and magnetic fields and the currents and particle velocities are Fourier analyzed in space and time according to $e^{i(kz - \omega t)}$ and will have the general form

$$F(r, z, t) = f(r) e^{i(kz - \omega t)} \quad (1)$$

All terms are assumed to have azimuthal symmetry. For a cold, collisionless plasma, the appropriate equation of motion for ions is

$$m_i \left(\frac{\partial \underline{v}_i}{\partial t} + \underline{v}_i \cdot \nabla \underline{v}_i \right) = e \underline{E} + e \frac{\underline{v}_i \times \underline{B}}{c} \quad (2a)$$

and for electrons,

$$m_e \frac{\partial \underline{v}_e}{\partial t} + \underline{v}_e \cdot \nabla \underline{v}_e = -e \underline{E} - e \frac{\underline{v}_e \times \underline{B}}{c} \quad (2b)$$

(All symbols are defined in appendix A and cgs-Gaussian units are used throughout this report.) A Fourier analysis is made in time according to equation (1). No zero-order velocities are assumed and $\underline{B} \cong \underline{B}_0 + \underline{B}(r)$. Then the higher order $\underline{v} \cdot \nabla \underline{v}$ and $\underline{v} \times \underline{B}(r)$ terms are dropped, and equations (2a) and (2b) become

$$-i\omega m_i \underline{v}_i(r) = e \underline{E}(r) + e \frac{[\underline{v}_i(r) \times \underline{B}_0]}{c} \quad (2c)$$

$$-i\omega m_e \underline{v}_e(r) = -e \underline{E}(r) - e \frac{[\underline{v}_e(r) \times \underline{B}_0]}{c} \quad (2d)$$

The plasma is assumed electrically neutral: $n_e = n_i = n(r)$. The current density in the plasma is given in terms of the macroscopic particle velocities as

$$\underline{j}(r) = n(r)e[\underline{v}_i(r) - \underline{v}_e(r)] \quad (3)$$

Equations (2c), (2d), and (3) are used to eliminate \underline{v}_i and \underline{v}_e to obtain $\underline{j}(r)$ as a function of $\underline{E}(r)$

$$\underline{j}(r) = \frac{\omega}{4\pi i} \underline{\underline{K}}'(r) \cdot \underline{E}(r) \quad (4)$$

The tensor $\underline{\underline{K}}'(r)$ is given as

$$\underline{\underline{K}}'(r) = \begin{pmatrix} S' & -iD' & 0 \\ iD' & S' & 0 \\ 0 & 0 & P' \end{pmatrix} \quad (5a)$$

in the coordinate system where the electric field is given as

$$\underline{E}(r) = \begin{pmatrix} E_r \\ E_\theta \\ E_z \end{pmatrix} \quad (5b)$$

$$\mathbf{R}' = -\frac{\Pi_i^2}{\omega^2} \left(\frac{\omega}{\omega + \Omega_i} \right) - \frac{\Pi_e^2}{\omega^2} \left(\frac{\omega}{\omega - \Omega_e} \right) \quad (5c)$$

$$\mathbf{L}' = -\frac{\Pi_i^2}{\omega^2} \left(\frac{\omega}{\omega - \Omega_i} \right) - \frac{\Pi_e^2}{\omega^2} \left(\frac{\omega}{\omega + \Omega_e} \right) \quad (5d)$$

$$\mathbf{P}' = -\frac{\Pi_i^2}{\omega^2} - \frac{\Pi_e^2}{\omega^2} \quad (5e)$$

$$\mathbf{S}' = \frac{1}{2} (\mathbf{R}' + \mathbf{L}') \quad (5f)$$

$$\mathbf{D}' = \frac{1}{2} (\mathbf{R}' - \mathbf{L}') \quad (5g)$$

where Π_e and Π_i are the electron and ion plasma frequencies, and Ω_e and Ω_i are the electron and ion cyclotron frequencies. Maxwell's equations are written as

$$\nabla \times \underline{\mathbf{E}} = -\frac{1}{c} \frac{\partial \underline{\mathbf{B}}}{\partial t} \quad (6a)$$

$$\nabla \times \underline{\mathbf{B}} = \frac{4\pi}{c} \underline{\mathbf{j}} + \frac{1}{c} \frac{\partial \underline{\mathbf{E}}}{\partial t} \quad (6b)$$

and are combined to give

$$\nabla \times \nabla \times \underline{\mathbf{E}} = \frac{4\pi i \omega}{c^2} \underline{\mathbf{j}} + \frac{\omega^2}{c^2} \underline{\mathbf{E}} \quad (6c)$$

where the Fourier analysis is again taken in time. Now, substituting equation (4) into equation (6c) yields

$$\nabla \times \nabla \times \underline{\mathbf{E}} = \frac{\omega^2}{c^2} \underline{\mathbf{K}}(\mathbf{r}) \cdot \underline{\mathbf{E}} \quad (7a)$$

where $\underline{K} = \underline{K}' + \underline{1}$. The three components of the vector equation (eq. (7a)) are

$$ik \left(\frac{\partial E_z}{\partial r} - ikE_r \right) - \frac{\omega^2}{c^2} (SE_r - iDE_\theta) = 0 \quad (7b)$$

$$k^2 E_\theta - \frac{\partial}{\partial r} \left(\frac{1}{r} \frac{\partial}{\partial r} rE_\theta \right) - \frac{\omega^2}{c^2} (iDE_r + SE_\theta) = 0 \quad (7c)$$

$$\frac{1}{r} \frac{\partial}{\partial r} \left[r \left(ikE_r - \frac{\partial E_z}{\partial r} \right) \right] - \frac{\omega^2}{c^2} PE_z = 0 \quad (7d)$$

where the Fourier analysis is now taken in the z-direction; E_r , E_θ , and E_z are functions of the radius r only; and $S = S' + 1$, $D = D'$, $P = P' + 1$, $R = R' + 1$, $L = L' + 1$.

Boundary Conditions

The boundary conditions that are to be imposed on the solutions to Maxwell's equations are as follows:

Plasma-vacuum-interface: The components of the tangential E-fields and B-fields must be continuous across a plasma-vacuum interface ($r = p$ and $r = \ell$):

$$\left(E_\theta^{\text{plasma}} \right)_{r=p, \ell} = \left(E_\theta^{\text{vac}} \right)_{r=p, \ell}$$

$$\left(E_z^{\text{plasma}} \right)_{r=p, \ell} = \left(E_z^{\text{vac}} \right)_{r=p, \ell}$$

or

$$\left. \begin{aligned} \left(B_\theta^{\text{plasma}} \right)_{r=p, \ell} &= \left(B_\theta^{\text{vac}} \right)_{r=p, \ell} \\ \left(ikE_r^{\text{plasma}} - \frac{\partial E_z^{\text{plasma}}}{\partial r} \right)_{r=p, \ell} &= \left(ikE_r^{\text{vac}} - \frac{\partial E_z^{\text{vac}}}{\partial r} \right)_{r=p, \ell} \end{aligned} \right\}$$

or

$$\left. \begin{aligned} \left(B_z^{\text{plasma}} \right)_{r=p, \ell} &= \left(B_z^{\text{vac}} \right)_{r=p, \ell} \\ \left(\frac{\partial E_\theta^{\text{plasma}}}{\partial r} \right)_{r=p, \ell} &= \left(\frac{\partial E_\theta^{\text{vac}}}{\partial r} \right)_{r=p, \ell} \end{aligned} \right\}$$

Current sheet at $r = s$: The components of the tangential E-fields and B_θ must be continuous at $r = s$. The component B_z is discontinuous by an amount $(4\pi/c)j^*$:

or

$$\left. \begin{aligned} \left(B_z^{\text{plasma}} \right)_{r=s} - \left(B_z^{\text{vac}} \right)_{r=s} &= \frac{4\pi}{c} j^* \\ \left(\frac{\partial E_\theta^{\text{plasma}}}{\partial r} \right)_{r=s} - \left(\frac{\partial E_\theta^{\text{vac}}}{\partial r} \right)_{r=s} &= \frac{4\pi i \omega}{c^2} j^* \end{aligned} \right\}$$

Vacuum Solutions

The solutions to Maxwell's equations in the vacuum regions (with displacement current neglected) are

$$\left. \begin{aligned} E_\theta &= b_1 I_1(kr) & (8a) \\ E_z &= c_1 I_0(kr) & (8b) \\ E_r &= -ic_1 I_1(kr) & (8c) \\ i \frac{\omega}{c} B_\theta &= \frac{\omega^2}{kc^2} c_1 I_1(kr) & (8d) \\ i \frac{\omega}{c} B_z &= kb_1 I_0(kr) & (8e) \end{aligned} \right\} 0 \leq r \leq \ell$$

$$E_{\theta} = d_1 I_1(kr) + d_2 K_1(kr) \quad (8f)$$

$$E_z = e_1 K_0(kr) \quad (8g)$$

$$E_r = ie_1 K_1(kr) \quad (8h)$$

$$i \frac{\omega}{c} B_{\theta} = \frac{-\omega^2}{kc^2} e_1 K_1(kr) \quad (8i)$$

$$i \frac{\omega}{c} B_z = kd_1 I_0(kr) - kd_2 K_0(kr) \quad (8j)$$

$p \leq r \leq s$

$$E_{\theta} = f_1 K_1(kr) \quad (8k)$$

$$E_z = e_1 K_0(kr) \quad (8l)$$

$$E_r = ie_1 K_1(kr) \quad (8m)$$

$$i \frac{\omega}{c} B_{\theta} = \frac{-\omega^2}{kc^2} e_1 K_1(kr) \quad (8n)$$

$$i \frac{\omega}{c} B_z = -kf_1 K_0(kr) \quad (8o)$$

$r \geq s$

where $b_1, c_1, d_1, d_2, e_1,$ and f_1 are constants of integration.

For the solid plasma cylinder ($\ell = 0$), the solutions for $0 \leq r \leq \ell$ are ignored.

Homogeneous Plasma (Solid or Annular)

For constant density ($n(r) = \text{Const}$), equations (7b) to (7d) are combined to give

$$(\mathcal{L}^2 - B\mathcal{L} + C)E_{\theta} = 0 \quad (9a)$$

$$iD \frac{\omega^2}{c^2} E_r = \left(k^2 - \mathcal{L} - \frac{\omega^2}{c^2} S \right) E_\theta = 0 \quad (9b)$$

$$ikPE_z = -\frac{1}{r} \frac{\partial}{\partial r} \left[r(SE_r - iDE_\theta) \right] \quad (9c)$$

where \mathcal{L} is an operator given by $\frac{\partial}{\partial r} \left(\frac{1}{r} \frac{\partial}{\partial r} r \right)$

$$B = \frac{k^2(P+S)}{S} - \frac{\omega^2}{c^2} P + \frac{\omega^2}{c^2} \frac{(D^2 - S^2)}{S} = \frac{k^2(P+S) - \frac{\omega^2}{c^2}(PS + RL)}{S}$$

$$C = \frac{P}{S} \left[k^4 - 2 \frac{\omega^2}{c^2} k^2 S + \frac{\omega^4}{c^4} (S^2 - D^2) \right] = \frac{P}{S} \left[\left(k^2 - \frac{\omega^2}{c^2} R \right) \left(k^2 - \frac{\omega^2}{c^2} L \right) \right]$$

For constant-density plasmas, B and C are not functions of the position variable r , and the fourth-order differential equation (9a) is factored into two second-order Bessel differential equations

$$\left(\mathcal{L} + \nu_1^2 \right) E_\theta = 0 \quad (10a)$$

$$\left(\mathcal{L} + \nu_2^2 \right) E_\theta = 0 \quad (10b)$$

where

$$\nu_1^2 = \frac{-B + \sqrt{B^2 - 4C}}{2} \quad (10c)$$

$$\nu_2^2 = \frac{-B - \sqrt{B^2 - 4C}}{2} \quad (10d)$$

From equations (10a) and (10b) four Bessel function solutions are obtained for E_θ : $J_1(\nu_1 r)$, $Y_1(\nu_1 r)$, $J_1(\nu_2 r)$, and $Y_1(\nu_2 r)$. The complete solution for E_θ is then

$$E_{\theta} = a_1 J_1(\nu_1 r) + a_3 Y_1(\nu_1 r) + a_2 J_1(\nu_2 r) + a_4 Y_1(\nu_2 r) \quad \text{for } \ell \leq r \leq p \quad (11a)$$

where a_1, a_2, a_3, a_4 are constants of integration. (It is assumed that ν_1^2 and ν_2^2 are both positive. When either ν_1^2 or ν_2^2 becomes negative, the appropriate Bessel functions should be substituted. See also appendix B.) From equation (9b)

$$\begin{aligned} iD \frac{\omega^2}{c^2} E_r &= \left(k^2 - \mathcal{L} - \frac{\omega^2}{c^2} S \right) E_{\theta} \\ &= \left(k^2 + \nu_1^2 - \frac{\omega^2}{c^2} S \right) [a_1 J_1(\nu_1 r) + a_3 Y_1(\nu_1 r)] \\ &\quad + \left(k^2 + \nu_2^2 - \frac{\omega^2}{c^2} S \right) [a_2 J_1(\nu_2 r) + a_4 Y_1(\nu_2 r)] \end{aligned}$$

is obtained, and from equation (9c),

$$ikPE_z = -\frac{1}{r} \frac{\partial}{\partial r} [r(SE_r - iDE_{\theta})]$$

and

$$\frac{\omega^2}{c^2} PE_z = \alpha \nu_1 [a_1 J_0(\nu_1 r) + a_3 Y_0(\nu_1 r)] + \beta \nu_2 [a_2 J_0(\nu_2 r) + a_4 Y_0(\nu_2 r)] \quad (11b)$$

are obtained. From $\nabla \times \underline{E} = -\frac{1}{c} \frac{\partial \underline{B}}{\partial t}$

$$i \frac{\omega}{c} B_z = \frac{1}{r} \frac{\partial}{\partial r} (rE_{\theta}) = \nu_1 [a_1 J_0(\nu_1 r) + a_3 Y_0(\nu_1 r)] + \nu_2 [a_2 J_0(\nu_2 r) + a_4 Y_0(\nu_2 r)] \quad (12a)$$

and

$$i \frac{\omega}{c} B_{\theta} = ikE_r - \frac{\partial E_z}{\partial r} = \alpha [a_1 J_1(\nu_1 r) + a_3 Y_1(\nu_1 r)] + \beta [a_2 J_1(\nu_2 r) + a_4 Y_1(\nu_2 r)] \quad (12b)$$

are obtained. Equations (11a), (11b), (12a), and (12b) are for $\ell \leq r \leq p$, where

$$\alpha = \frac{S(k^2 + \nu_1^2) - RL \frac{\omega^2}{c^2}}{kD}$$

$$\beta = \frac{S(k^2 + \nu_1^2) - RL \frac{\omega^2}{c^2}}{kD}$$

The constants a_1, a_2, a_3, a_4 must be determined from boundary conditions. For the solid cylinder of plasma, $\ell = 0$, and a_3 and $a_4 = 0$ because $E_{\theta}^{\text{plasma}}$ is finite at $r = 0$.

Power Transfer to Homogeneous Plasma

When the aforementioned boundary conditions are applied to the constant-density solutions (solid or annular), a system of simultaneous equations is obtained for the coefficients in equations (8), (11), and (12). These simultaneous equations can be used to solve for $a_1, a_2, a_3, a_4, d_1, d_2, e_1$, and f_1 . Calculation of the power absorbed by the plasma requires the value of the azimuthal electric field at $r = s$ (ref. 1). This value can be written as

$$\left[E_{\theta}^{\text{vac}}(k) \right]_{r=s} = f_1 K_1(ks) \quad (13)$$

The electric field $\left[E_{\theta}^{\text{vac}}(k) \right]_{r=s}$ is the field at the position of the current sheet for an infinitely long current sheet. What is actually needed is an expression for $(E_{\theta})_{r=s}$ for a finite-length current sheet of length $2a$ with a current density

$$\underline{j}^* = j^* e^{i(k_0 z - \omega t)} \hat{\theta} \quad (-a \leq z \leq a) \quad (14a)$$

$$\underline{j}^* = 0 \quad |z| > a \quad (14b)$$

For a finite-length current sheet, $(E_\theta)_{r=s}$ is obtained as follows (ref. 1): The current-sheet density \underline{j}^* from equations (14) is decomposed into its Fourier integral spectrum, so that

$$\underline{j}^* = \hat{\theta} j^* \int_{-\infty}^{\infty} \frac{\sin(k - k_0)a}{\pi(k - k_0)} e^{i(kz - \omega t)} dk \quad (15)$$

The electric field for the finite-length current sheet can then be represented as the sum (integral) of the electric fields of a continuous set of infinitely long current sheets, each having the infinitesimal amplitude

$$dj = j^* \frac{\sin(k - k_0)a}{\pi(k - k_0)} e^{i(kz - \omega t)} dk$$

so that

$$(E_\theta)_{r=s} = \int_{-\infty}^{\infty} \left[E_\theta^{\text{vac}}(k) \right]_{r=s} \frac{\sin(k - k_0)a}{\pi(k - k_0)} e^{i(kz - \omega t)} dk \quad (16)$$

Equation (16) was integrated by contour integration (as in ref. 1) to give the following result for a right-running current-sheet wave:

$$(E_\theta)_{r=s} = j^* \sum_{n=1}^{\infty} R_n e^{ik_0 z - i\omega t} \left[\frac{1 - e^{-i(k_0 - k_n)(z+a)}}{k_0 - k_n} \right] \quad -a \leq z \leq a \quad (17a)$$

where

$$R_n = \frac{\left[(k - k_n) \left(E_\theta^{\text{vac}} \right)_{r=s} \right]_{k=k_n}}{j^*} \quad (17b)$$

(It should be noted that the R_n defined in eq. (17b) is not the same as the R_n defined on p. 96 of ref. 1.)

The values $k = k_n$ are the values of k where $\left(E_\theta^{\text{vac}} \right)_{r=s}$ becomes infinite. They correspond to the poles of the integrand in equation (16). The k_n 's are the wave numbers for the natural modes of the plasma column in a vacuum. This suggests that each term in the sum in equation (17a) is the electric field of the n^{th} natural mode.

The component of the electric field $\left(E_\theta \right)_{r=s}$, which stems from power absorption in the plasma, tends to decelerate charge carriers in the current sheet. Thus, the instantaneous power per unit area required to drive the surface current against the electric field at $r = s$ is $-\left[E_\theta \cdot j^* \right]_{r=s}$. Therefore, the time-averaged power transfer to the plasma is obtained by integrating over the total surface of the current sheet as follows:

$$P_t = \frac{1}{2} \text{Re} \int_{-a}^a - \left(E_\theta \right)_{r=s} \cdot j^* e^{-ik_0 z + i\omega t} 2\pi s dz \quad (18)$$

Integrating equation (18) gives

$$P_t = (2\pi a s) (-iaj^*)^2 \sum_{n=1}^{\infty} R_n S_r(\eta_n) \quad (19a)$$

or

$$P_t = (2\pi a^2) j^*{}^2 \sum_{n=1}^{\infty} R_n' S_r(\eta_n) \quad (19b)$$

where

$$S_r(\eta_n) = \frac{2(1 - \cos \eta_n)}{\eta_n^2} \quad (19c)$$

$$\eta_n = 2(k_o - k_n)a \quad (19d)$$

and

$$R'_n = -isR_n \quad (19e)$$

From equations (13) and (17b) and from the fact that the denominator of $(E_\theta^{\text{vac}})_{r=s}$ (hereinafter denoted as $\Gamma_1(k)$) must be zero, R'_n can be calculated.

R'_n for Homogeneous Plasma

For the simpler case of the solid cylinder ($\ell = 0$) the expression for R'_n is

$$R'_n = \left((k - k_n) \left(\frac{4\pi\omega}{c^2} \right) \left[\frac{s^2 K_1^2(ks)}{kpK_0(kp)K_1(kp)} \right] \frac{\left\{ \alpha [PJ_1(\nu_1 p) + \gamma \nu_1 p J_0(\nu_1 p)] J_1(\nu_2 p) - \beta [PJ_1(\nu_2 p) + \gamma \nu_2 p J_0(\nu_2 p)] J_1(\nu_1 p) \right\}}{\Gamma_1(k)} \right)_{\substack{k=k_n \\ \Gamma_1=0}} \quad (20)$$

where

$$\gamma = \frac{K_1(kp)}{kpK_0(kp)}$$

The functions $\Gamma_1(k)$ are given in appendix B. The indeterminacy in equation (20) may be eliminated by L'Hospital's rule, so that

$$\lim_{k \rightarrow k_n} \frac{k - k_n}{\Gamma_1(k)} = \left[\frac{d\Gamma_1(k)}{dk} \right]_{k=k_n}^{-1} \quad (21)$$

For the case of the hollow cylinder of plasma,

$$R'_n = \left((k - k_n) \left(\frac{4\pi\omega}{c^2} \right) \frac{s^2 [K_1(ks)]^2}{kpK_0(kp)K_1(kp)} \frac{\left\{ [-\bar{M}_{41} J_1(\nu_1 p) + \bar{M}_{42} J_1(\nu_2 p) - \bar{M}_{43} Y_1(\nu_1 p) + \bar{M}_{44} Y_1(\nu_2 p)] \right\}}{\Gamma_2(k)} \right)_{\substack{k=k_n \\ \Gamma_2=0}} \quad (22)$$

where $\Gamma_2(k) = \det M$; and \overline{M}_{41} , \overline{M}_{42} , \overline{M}_{43} , \overline{M}_{44} are the minors of the matrix M , which is also given in appendix B. Again, the determinant M becomes zero when $k = k_n$ and the indeterminacy is eliminated by L'Hospital's rule. The values ν_{1n} , ν_{2n} , and k_n , when $\Gamma_2 = 0$, are the values obtained for the natural modes of oscillation of an infinitely long plasma column surrounded by a vacuum. Thus each term in the sum of equation (19b) may be thought of as the power transmitted by a single natural mode of the plasma.

Inhomogeneous Plasma

If, as in an inhomogeneous plasma, $n(r)$ does not equal a constant, equations (7b) to (7d) combine to give a lengthy, unfactorable fourth-order differential equation for E_θ , which must be solved by numerical means. If the 1 is neglected in the terms R , L , S , and P (which is the same as neglecting displacement current), R , L , S , P , or D can be written in the form $Q = Q_0 g(r)$, where Q_0 is the value of R , L , S , P , D , or n at $r = 0$, and $g(r)$ is the density distribution function so that $n(r) = n_0 g(r)$. Thus, when displacement current is neglected, the differential equations for the electric-field components in an inhomogeneous plasma are

$$\begin{aligned}
& \frac{\partial^4 E_\theta}{\partial r^4} + \frac{\partial^3 E_\theta}{\partial r^3} \left(\frac{2}{r} - \frac{g'}{g} \right) + \frac{\partial^2 E_\theta}{\partial r^2} \left\{ -\frac{3}{r^2} - \frac{2}{r} \frac{g'}{g} + \frac{P_0}{S_0} \left(-k^2 + \frac{\omega^2}{c^2} S_0 g \right) \right. \\
& \quad \left. + \frac{1}{S_0} \left[-k^2 S_0 + \frac{\omega^2}{c^2} (S_0^2 - D_0^2) g \right] \right\} + \frac{\partial E_\theta}{\partial r} \left(k^2 \frac{g'}{g} + \frac{1}{r^2} \frac{g'}{g} + \frac{3}{r^3} - \frac{\omega^2}{c^2} \left(\frac{D_0^2}{S_0} - S_0 \right) g' \right. \\
& \quad \left. + \frac{1}{r} \left\{ \frac{P_0}{S_0} \left(-k^2 + \frac{\omega^2}{c^2} S_0 g \right) + \frac{1}{S_0} \left[-k^2 S_0 + \frac{\omega^2}{c^2} (S_0^2 - D_0^2) g \right] \right\} \right) \\
& \quad + E_\theta \left\{ \frac{P_0}{S_0} \left[\left(k^4 - \frac{2\omega^2}{c^2} k^2 S_0 g \right) + \frac{\omega^4}{c^4} (S_0^2 - D_0^2) g^2 \right] - \frac{\omega^2}{c^2} \left(S_0 - \frac{D_0^2}{S_0} \right) \left(\frac{g'^2}{g} - g'' + \frac{g}{r^2} \right) \right. \\
& \quad \left. + \frac{1}{r} k^2 \frac{g'}{g} + \frac{k^2}{r^2} - \frac{1}{r^2} \frac{P_0}{S_0} \left(-k^2 + \frac{\omega^2}{c^2} S_0 g \right) - \frac{1}{r^3} \frac{g'}{g} - \frac{3}{r^4} \right\} = 0 \tag{23a}
\end{aligned}$$

$$\frac{i\omega}{c} B_\theta = ikE_r - \frac{\partial E_z}{\partial r} = -\frac{S_o}{kD_o} \left\{ \left[-k^2 + \frac{\omega^2}{c^2} \left(S_o - \frac{D_o^2}{S_o} \right) g - \frac{1}{r^2} \right] E_\theta + \frac{1}{r} \frac{\partial E_\theta}{\partial r} + \frac{\partial^2 E_\theta}{\partial r^2} \right\} \quad (23b)$$

$$E_z = \frac{-c^2 S_o}{\omega^2 k D_o P_o g} \left\{ \frac{\partial^3 E_\theta}{\partial r^3} + \frac{2}{r} \frac{\partial^2 E_\theta}{\partial r^2} + \frac{\partial E_\theta}{\partial r} \left[-k^2 - \frac{1}{r^2} + \frac{\omega^2}{c^2} \left(S_o - \frac{D_o^2}{S_o} \right) g \right] + E_\theta \left[-\frac{k^2}{r} + \frac{1}{r^3} + \frac{\omega^2}{c^2} \left(S_o - \frac{D_o^2}{S_o} \right) \left(g' + \frac{g}{r} \right) \right] \right\} \quad (23c)$$

where $g' = dg/dr$ and $g'' = d^2g/dr^2$. These equations must then be solved numerically. The electric and magnetic fields in the plasma are denoted as $E_r(r)$, $E_\theta(r)$, and $E_z(r)$, and $B_r(r)$, $B_\theta(r)$, and $B_z(r)$. Applying boundary conditions gives the following expression for the θ -component of the electric field of an infinite-length current sheet at $r = s$:

$$\left[E_\theta^{\text{vac}}(k) \right]_{r=s} = \frac{4\pi i \omega}{c^2} j^* s K_1(ks) \left\{ I_1(ks) + \frac{K_1(ks) \left[I_1(kp) \left(\frac{\partial E_\theta}{\partial r} \right)_{r=p} - k I_1'(kp) (E_\theta)_{r=p} \right]}{k K_1'(kp) (E_\theta)_{r=p} - K_1(kp) \left(\frac{\partial E_\theta}{\partial r} \right)_{r=p}} \right\} \quad (24)$$

with the additional constraint that

$$\Delta = \frac{-\omega^2}{kc^2} K_1(kp) (E_z)_{r=p} + K_0(kp) \left(\frac{i\omega}{c} \right) (B_\theta)_{r=p} = 0 \quad (25)$$

This additional constraint comes from the E_z and B_θ boundary conditions. Since $E_z(r)$ and $B_\theta(r)$ are functions of $E_\theta(r)$, equation (25) acts as a boundary condition for $E_\theta(r)$ at $r = p$.

Because of the particular numerical technique (see appendix C) used to solve for $E_\theta(r)$, it is necessary to know the value of $E_\theta(r)$ and its first three derivatives at $r = 0$. Because $\left[E_\theta(r) \right]_{r=0}$ is zero, and $E_\theta(r)$ is asymmetric about $r = 0$, $\left[E_\theta(r) \right]_{r=0} = 0$ and

$\left[\partial^2 E_\theta(r) / \partial r^2 \right]_{r=0} = 0$. From equation (24) it can be seen that only the ratio

$\left\{ E_\theta(r) / \left[\partial E_\theta(r) / \partial r \right] \right\}_{r=p}$ is required to calculate $\left(E_\theta^{\text{vac}} \right)_{r=s}$. Since only the ratio

$\left\{ E_\theta(r) / \left[\partial E_\theta(r) / \partial r \right] \right\}_{r=p}$ is needed and the differential equation for E_θ is linear, only

the ratio $\left\{ \left[\frac{\partial E_\theta(r)}{\partial r} \right] / \left[\frac{\partial^3 E_\theta(r)}{\partial r^3} \right] \right\}_{r=0}$ needs to be specified. Then, choosing

$\left[\frac{\partial E_\theta(r)}{\partial r} \right]_{r=0} = 1$ leaves only $\left[\frac{\partial^3 E_\theta(r)}{\partial r^3} \right]_{r=0}$ to be determined by the following iteration process. For r near zero, the terms in equation (23a) that involve the density-distribution function are small, and the solutions behave like Bessel functions. Hence, $\left[\frac{\partial^3 E_\theta(r)}{\partial r^3} \right]_{r=0}$ is first computed for the case of a constant-density plasma $n = n_0$. This value is then used as a first guess for the variable-density value. The values of $E_\theta(r)$, $E_r(r)$, and $E_z(r)$ at p are then computed, and the test of equation (25) is applied. If $\Delta \neq 0$, a Newton-Raphson formula is used to find a new value for $\left[\frac{\partial^3 E_\theta(r)}{\partial r^3} \right]_{r=0}$ and Δ is again computed. This iteration continues until the change in $\left[\frac{\partial^3 E_\theta(r)}{\partial r^3} \right]_{r=0}$ from one iteration to the next is must less than $\left[\frac{\partial^3 E_\theta(r)}{\partial r^3} \right]_{r=0}$.

Once the values of $\left[E_\theta(r) \right]_{r=p}$ and $\left[\frac{\partial E_\theta(r)}{\partial r} \right]_{r=p}$ have been determined under the constraint $\Delta = 0$, equation (24) can be used in equations (16). Now the same procedure used in deriving equations (17a) to (19c) may be applied to the variable-density case. The new expression for R'_n is

$$R'_n = \left\{ \frac{-4\pi\omega}{c^2} \frac{s^2 [K_1(ks)]^2 \left[I_1(kp) \left(\frac{\partial E_\theta}{\partial r} \right)_{r=p} - k I_1'(kp) (E_\theta)_{r=p} \right]}{\frac{d\Gamma_3}{dk}} \right\}_{\substack{k=k_n \\ \Gamma_3=0}} \quad (26)$$

where

$$\Gamma_3(k) = k K_1'(kp) (E_\theta)_{r=p} - K_1(kp) \left(\frac{\partial E_\theta}{\partial r} \right)_{r=p} \quad (27)$$

RESULTS AND DISCUSSION

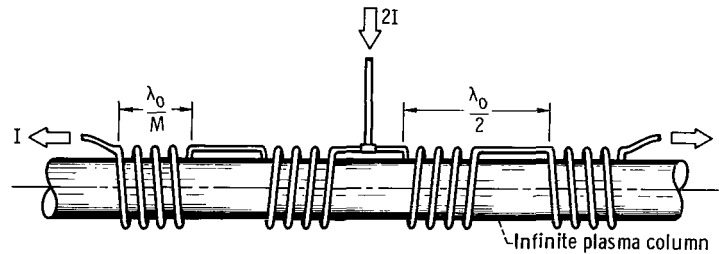
From the previous section, the independent variables in an ion cyclotron wave experiment included sheet-current radius, wavelength, and overall length; plasma radius, density, and radial density profile; steady magnetic field; and generator frequency. Also important are other effects, such as axial variations of the magnetic field, ion and

electron temperature, and damping phenomena. However, these effects have not been included because they entail more complex theory, and their effects can be minimized through proper design of the experiment. Conditions for which temperature and damping effects can be neglected are discussed briefly in this section. The intent here is to present results for a theoretical model of ion cyclotron wave generation that can be reasonably approached in the laboratory.

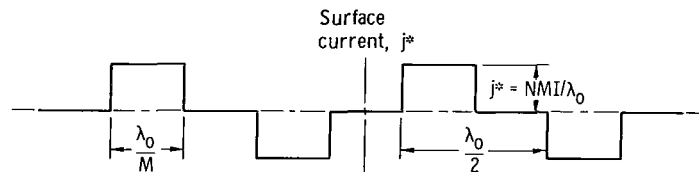
Current-Sheet Representation

Figure 2(a) shows a Stix-type (ref. 1) radiofrequency coil that may be used to produce a current sheet that varies approximately as $j^* e^{i(k_0 z - \omega t)}$, where $k_0 = 2\pi/\lambda$. If N is the number of turns in each of the four sections of the coil, I is the peak radiofrequency current flowing through the coil, and λ_0/M is the length of each section, the equivalent rectangular current sheet can be represented as shown in figure 2(b). The rectangular current sheet can be represented by a Fourier series with coefficients given as $|A_m| = \frac{4NMI}{m\pi\lambda_0} \sin \frac{m\pi}{M}$, where $m = 1, 3, 5$, etc. Since power transfer is proportional to $|A_m|^2$, the fundamental ($m = 1$) is usually sufficient for power calculations. Thus, the rectangular current sheet is represented as

$$j^* = \frac{4NMI}{\pi\lambda_0} \sin \frac{\pi}{M} \tag{28}$$



(a) Radiofrequency coil.



(b) Current-sheet representation.

Figure 2. - Radiofrequency-coil configuration and equivalent current sheet.

Substituting this last expression into equation (19b) yields the power transfer from the fundamental component of the Stix coil:

$$P_t = 2\pi a^2 \left(\frac{4NMI}{\pi \lambda_0} \sin \frac{\pi}{M} \right)^2 \sum_n R'_n S_r(\eta_n) \quad (29)$$

Equation (29) can be used to compute power transfer for either the constant- or variable-density case, and for any value of N , M , λ_0 , I , a , p , s , n_e , ω , and Ω_i . Aside from some practical electric circuit problems that are discussed briefly in this section, it is obvious from equation (29) and from the expressions for R'_n (eqs. (20), (22), and (26)) how the values of N , M , a , and ω will affect power transfer. Hence, typical values of $N = M = 4$, $a = 45$ centimeters, and $\omega/2\pi = 6.5$ megahertz are used for all calculations. The coil is 2 wavelengths long. Although the effects of coil wavelength and radius are examined in this section, for illustrative purposes most of the results are presented for $s = 10$ centimeters and $\lambda_0 = 45$ centimeters. The aforementioned values of the parameters N , M , a , and ω are used in equation (29) to obtain

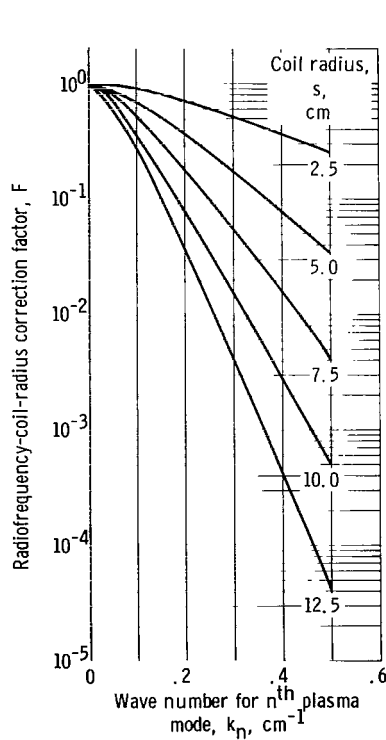


Figure 3. - Radiofrequency-coil-radius correction factor as function of wave number for n^{th} plasma mode.

$$\frac{P_t}{\text{watts}} = 1.17 \times 10^{15} \left(\frac{I}{\text{amperes}} \right)^2 \left[\frac{\sum_n R'_n S_r(\eta_n)}{\text{statohms}} \right] \quad (30)$$

The effects of each independent variable on power transfer are discussed in the following paragraphs.

Coil Radius

The effect of coil radius s on P_t is given entirely by the term

$$F(k_n s) = (k_n s)^2 K_1(k_n s)^2$$

which appears in R'_n (eqs. (20), (22), and (26)). This factor $F(k_n s)$, is presented in figure 3 as a function of k_n with s as a parameter. The term R'_n (for $s = 10.0$ centi-

meters) may be corrected to any value of the coil radius by multiplying R'_n (for $s = 10.0$ cm) by the ratio $F(k_n s)/F(10k_n)$. However, approximate corrections to P_t can be made simply by multiplying P_t (for $s = 10.0$) by $F(k_o s)/F(10k_o)$. It may be seen from $F(k_n s)$ that, for a given coil wavelength, it is desirable to make s as small as possible but subject to the restriction $s \geq p$.

Frequency

The function R'_n is also directly proportional to ω (see eqs. (20), (22), and (26)). However, to increase the power transfer to the plasma merely by increasing the fre-

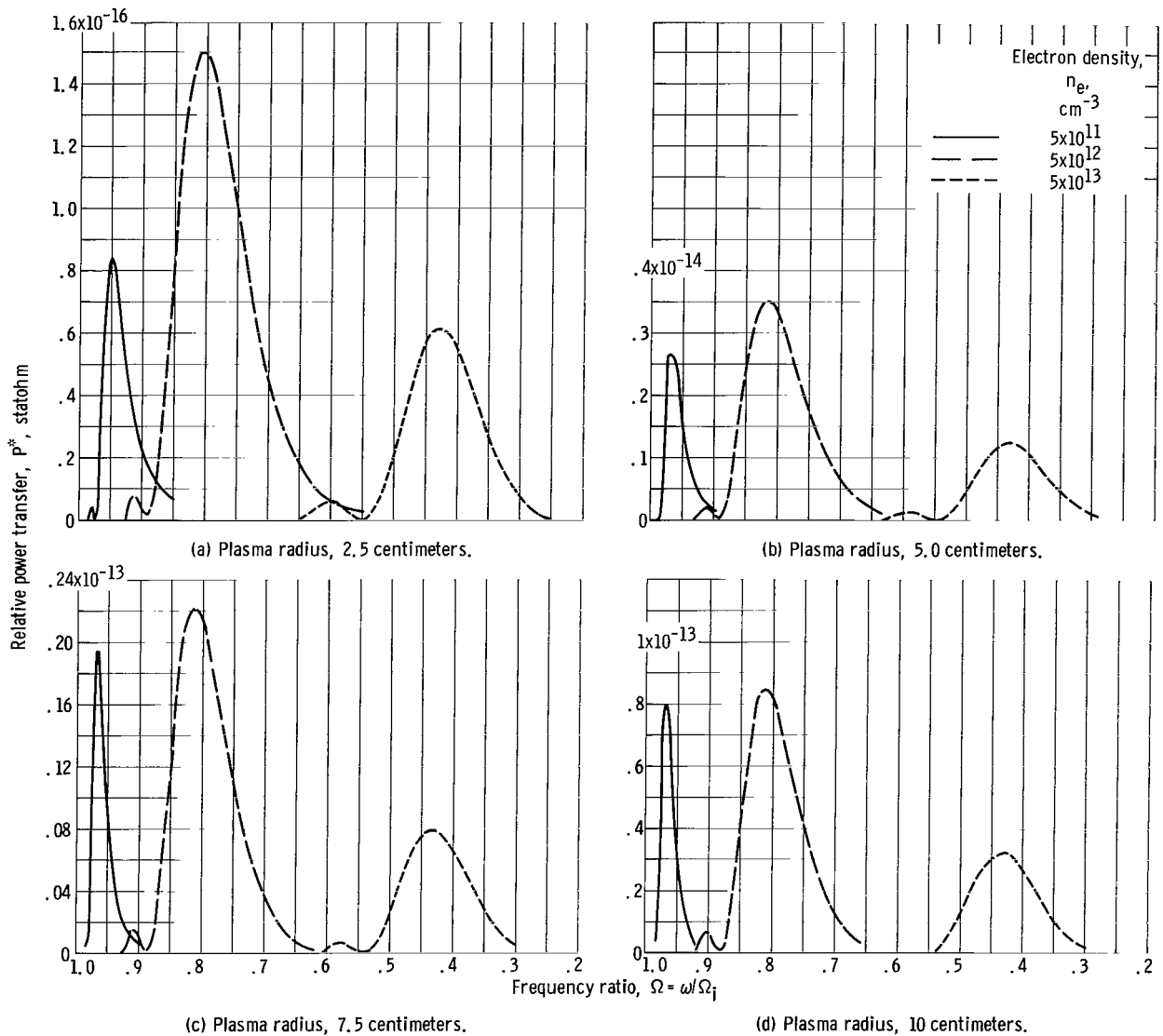


Figure 4. - Relative power transfer as function of frequency ratio.

quency requires redesign of the coil system, since the radiofrequency coil impedance increases and causes high electrostatic voltages. Experimentally, the coil is operated so close to its natural frequency that further increases in ω would introduce severe impedance-matching problems. In addition, larger, steady B-fields are required since peak power occurs at a given value of $\Omega = \omega/\Omega_i$.

Solid Cylinder of Constant-Density Plasma

Figure 4 presents plots of relative power

$$P^* = \frac{P_t}{2\pi a^2 j^2} = \sum_n R_n' S_r(\eta_n)$$

as a function of Ω for all combinations of the following plasma radii and densities: $p = 2.5, 5.0, 7.5,$ and 10.0 centimeters, and $n_e = 5 \times 10^{11}, 5 \times 10^{12},$ and 5×10^{13} per cubic centimeter. An interpretation of these results and a discussion of significant trends follow. All the curves of P^* as a function of Ω exhibit a peak (resonance). The value of Ω at the peak, as well as at the half power points, depends primarily on electron density. For higher densities ($n_o = 5 \times 10^{13} \text{ cm}^{-3}$), Ω at the peak is lower, and vice versa. Smaller dependencies on plasma radius and on current-sheet wavelength are discussed in more detail later.

In general, the shape factor $S_r(\eta_n)$ for the $n = 1$ mode controls the shape of these curves. The shape factor is given as a function of η_n in figure 5.

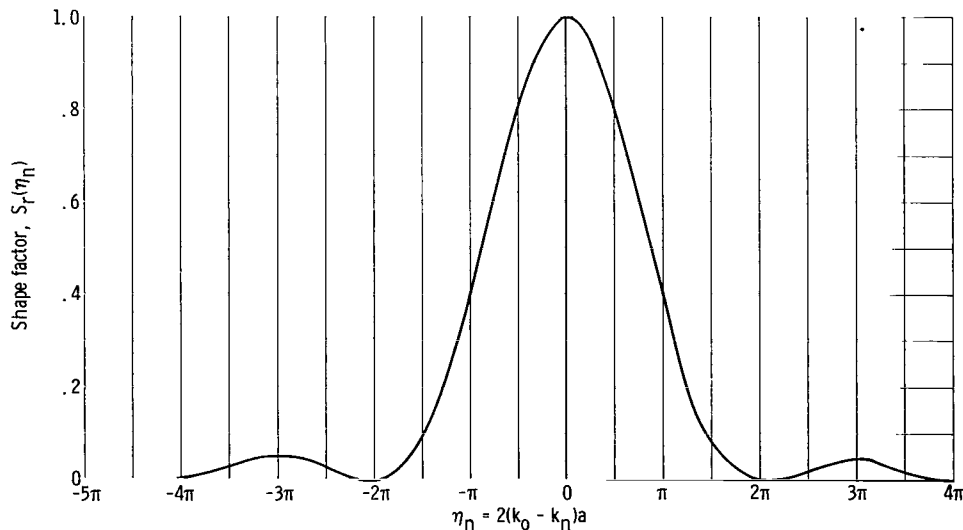


Figure 5. - Shape factor $S_r(\eta_n)$ as function of η_n .

Plasma density. - An examination of figure 4 reveals that the optimum density for power transfer to the plasma wave is about 5×10^{12} per cubic centimeter or slightly less. This optimum density does not seem to depend strongly on plasma radius. In the section Variable Density and Annular Plasmas, it will be shown that power transfer is substantially lower than the maximum for $n_e < 10^{11}$ per cubic centimeter or $n_e > 10^{14}$ per cubic centimeter.

Current-sheet wavelength. - The 45-centimeter wavelength chosen for most of the calculations does not necessarily represent the optimum wavelength for efficient power transfer. As a result, some calculations were made for current sheets 2 wavelengths long with wavelengths of 25, 35, and 55 centimeters. If it is assumed that I, N, and M are held constant, maximum power occurs when P^* is a maximum. Tables I and II summarize the results of these calculations by presenting P^*_{max} and the corresponding value of Ω for all coil wavelengths, plasma radii, and densities for which constant-density calculations were made.

Several features of table I should be explained, the first of which is that the optimum wavelength for any given combination of plasma radius and density depends on the actual

TABLE I. - DEPENDENCE OF MAXIMUM RELATIVE POWER
TRANSFER ON PLASMA RADIUS, ELECTRON DENSITY,
AND CURRENT-SHEET WAVELENGTH

[Surface current-sheet radius, 10.0 cm.]

Plasma column outer radius, p, cm	Electron density, n_e , cm^{-3}	Wavelength of surface-current sheet, λ_0 , cm			
		25	35	45	55
		Maximum relative power transfer, P^*_{max} , statohm			
2.5	5×10^{11}	0.87×10^{-16}	0.97×10^{-16}	0.84×10^{-16}	0.65×10^{-16}
	5×10^{12}	1.97	1.98	1.50	1.05
	5×10^{13}	1.35	1.03	.612	.385
5.0	5×10^{11}	3.08×10^{-15}	3.24×10^{-15}	2.64×10^{-15}	2.10×10^{-15}
	5×10^{12}	5.03	4.70	3.50	2.44
	5×10^{13}	3.08	2.16	1.24	.726
7.5	5×10^{11}	2.58×10^{-14}	2.44×10^{-14}	1.95×10^{-14}	1.48×10^{-14}
	5×10^{12}	3.57	3.09	2.21	1.49
	5×10^{13}	2.41	1.45	.79	.45
10.0	5×10^{11}	1.32×10^{-13}	1.08×10^{-13}	0.80×10^{-13}	0.59×10^{-13}
	5×10^{12}	1.67	1.27	.85	.56
	5×10^{13}	1.17	.68	.32	.17

TABLE II. - RATIO OF WAVE FREQUENCY TO ION CYCLOTRON FREQUENCY AT MAXIMUM RELATIVE POWER TRANSFER AS FUNCTION OF PLASMA RADIUS, ELECTRON DENSITY, AND CURRENT-SHEET WAVELENGTH

Plasma column outer radius, p, cm	Electron density, n_e , cm^{-3}	Wavelength of surface-current sheet, λ_0 , cm			
		25	35	45	55
		Frequency ratio, $\Omega = \omega/\Omega_i$			
2.5	5×10^{11}	0.980	0.969	0.950	0.930
	5×10^{12}	.91	.86	.80	.75
	5×10^{13}	.62	.50	.43	.36
5.0	5×10^{11}	0.987	0.978	0.967	0.953
	5×10^{12}	.91	.86	.81	.76
	5×10^{13}	.62	.51	.43	.37
7.5	5×10^{11}	0.988	0.980	0.969	0.958
	5×10^{12}	.91	.86	.81	.76
	5×10^{13}	.62	.51	.43	.37
10.0	5×10^{11}	0.988	0.980	0.970	0.958
	5×10^{12}	.91	.86	.81	.76
	5×10^{13}	.62	.51	.43	.37

values of p and n_e . The optimum wavelength is shorter for high densities and large plasma radii. The optimum value of P_{max}^* as a function of λ_0 is not always evident from the table, since finding this optimum would require calculations for λ_0 less than 25 centimeters. For such short wavelengths and for a given density, the value of Ω at P_{max}^* is closer to 1 so that it becomes increasingly difficult to satisfy the conditions for which cold-plasma theory applies. However, in determining the proper wavelength for the current sheet, other factors must be taken into account. One of these is ohmic losses in the current sheet (coil). For example, increasing the wavelength, and thereby increasing ohmic losses to get an increase in power transfer for a given current, makes little sense if the change in ohmic loss exceeds the increase in power transfer. Second, ion cyclotron wave experiments have been plagued by an undesired coupling of power to the plasma. This coupling was a result of high E_z fields in the plasma, which are produced by the voltages across

the coil (ref. 3). This undesired coupling has been greatly reduced by the use of a properly grounded electrostatic Faraday shield between the current sheet and the plasma. Since the voltage across the current sheet for a given current is determined primarily by the inductance of the current sheet, it may not always be desirable to change the wavelength (if it should increase inductance) to get increased power transfer. Furthermore, higher coil voltages can cause arcing problems between the coil and the ground points.

Plasma radius. - Figure 6(a) shows the maximum value of P^* as a function of plasma radius for several densities ($\lambda_0 = 45$ cm, $s = 10.0$ cm). This power transfer P_{max}^* increases approximately as the 4.5 power of the plasma radius. Examination of table I shows that this radius effect changes slightly with λ_0 . Figure 6(b) shows P_{max}^* as a function of plasma radius for the case where s equals p ($\lambda_0 = 45$ cm). In this case P_{max}^* increases as the 3.5 power of the plasma radius. These curves reveal that the plasma radius has an extremely large effect on power transfer.

Dispersion relation for finite electron mass. - For experimentalists, it is useful to have a simple expression relating the wavelength of the plasma wave to Ω . Using basi-

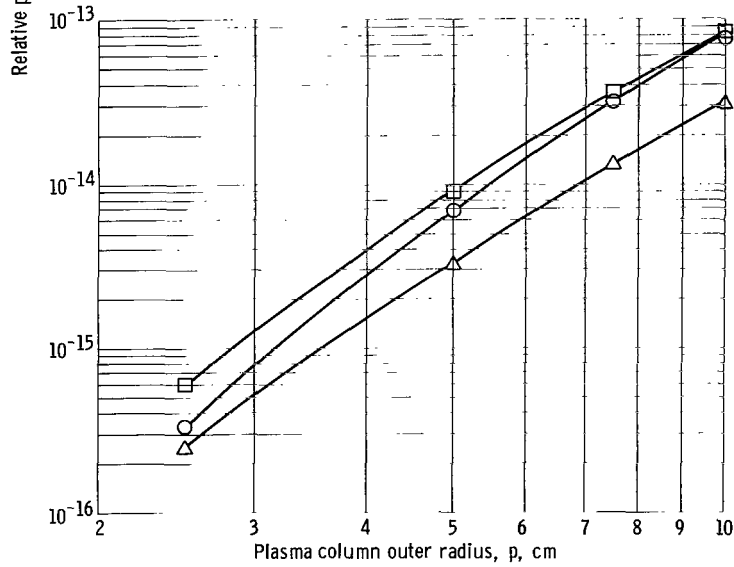
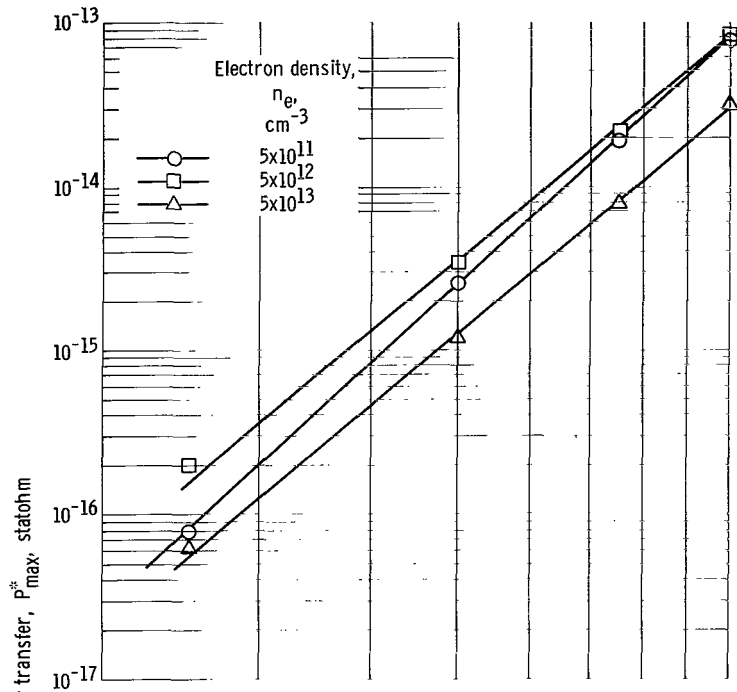


Figure 6. - Relative power transfer as function of plasma radius. Surface current-sheet wavelength, 45 centimeters.

cally the same model for the plasma as described in this report, but making the additional assumption that the mass of the electron was zero, Stix (ref. 1) derived the following dispersion law that holds, approximately, for all plasma modes:

$$\Omega^2 = \frac{1}{1 + \frac{\lambda_n^2}{4\pi^2} \left(\frac{\Pi_i^2}{c^2} \right)} \quad (31)$$

For densities less than 10^{13} per cubic centimeter and for plasma radii less than 5.0 centimeters, equation (10c) may be simplified. Let ν_1 for the n^{th} mode be denoted as ν_{1n} . If $B^2 \gg 4C$, then

$$\nu_{1n}^2 \approx -B \approx -\frac{P}{S} \left(k^2 - \frac{\omega^2}{c^2} S \right)$$

and for $m_e \neq 0$,

$$\Omega^2 \approx \frac{1}{1 + \frac{\lambda_n^2}{4\pi^2} \left(\frac{m_e}{m_i} \nu_{1n}^2 + \frac{\Pi_i^2}{c^2} \right)} \quad (32)$$

When boundary conditions were applied to the plasma model, the computer solutions showed that $J_1(\nu_1 p) \approx 0$ when $\Gamma = 0$. If the arguments of $J_1(\nu_1 p)$ are denoted as X_n when $\Gamma = 0$, $\nu_{1n}^2 = (X_n/p)^2$. Thus, the relation obtained for the condition $\Gamma = 0$ is

$$\Omega^2 \approx \frac{1}{1 + \frac{\lambda_n^2}{4\pi^2} \left[\frac{m_e}{m_i} \left(\frac{X_n}{p} \right)^2 + \frac{\Pi_i^2}{c^2} \right]} \quad (33)$$

where $X_n = 3.83, 7.00, 10.15, 13.3, 16.5$, etc., for $n = 1, 2, 3, 4, 5$, etc.

The finite-electron-mass dispersion equation (eq. (33)) differs from the zero-electron-mass dispersion equation (eq. (31)) for small values of p , but the two equations are identical in the limit of large plasma radius or high density (i.e., $\Pi_e^2/c^2 \gg (X_n/p)^2$). Equations (31) and (33) are plotted in figure 7.

As noted before, the values of ν_{1n} and $\lambda_n(k_n)$ when $\Gamma = 0$ are the values obtained

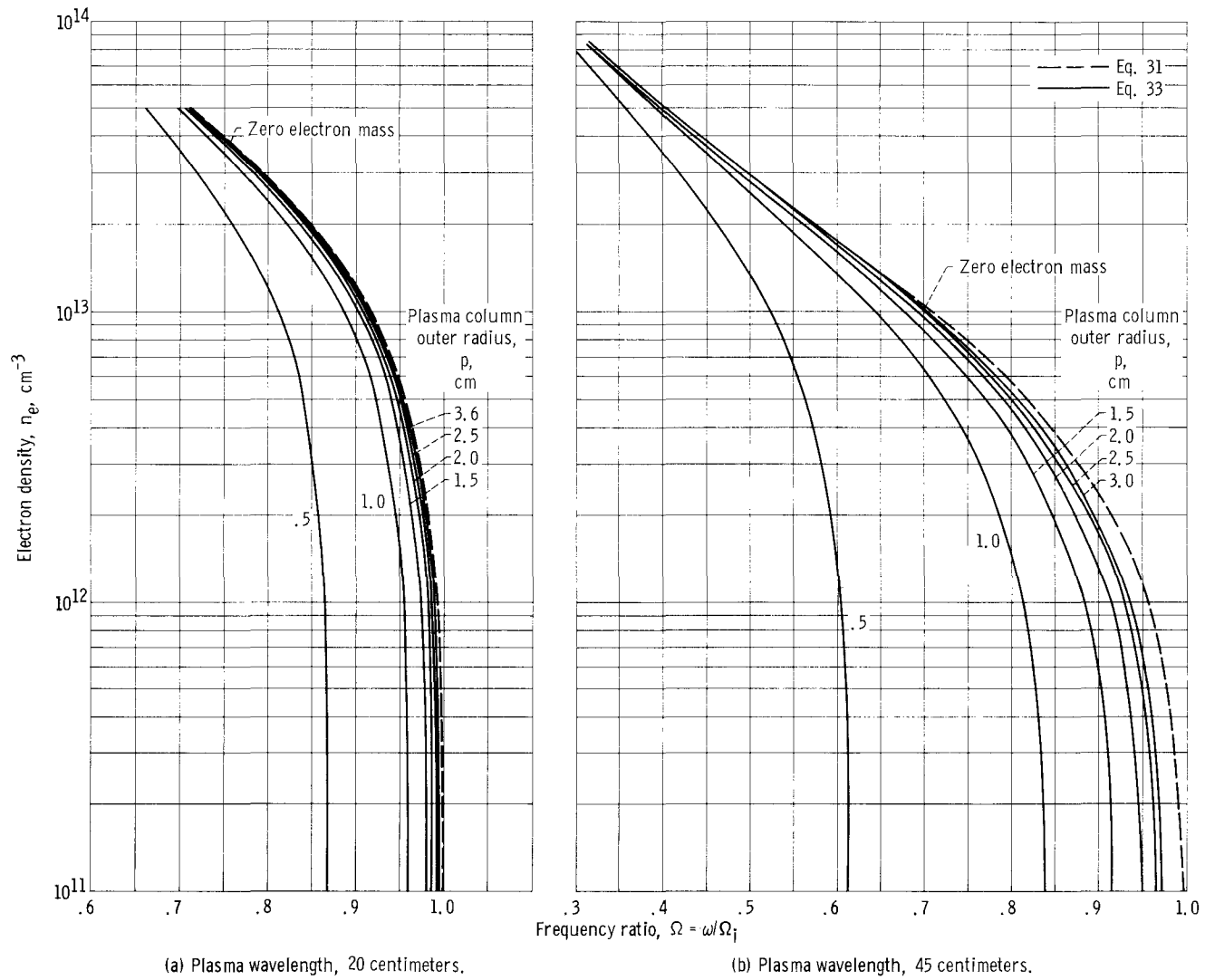
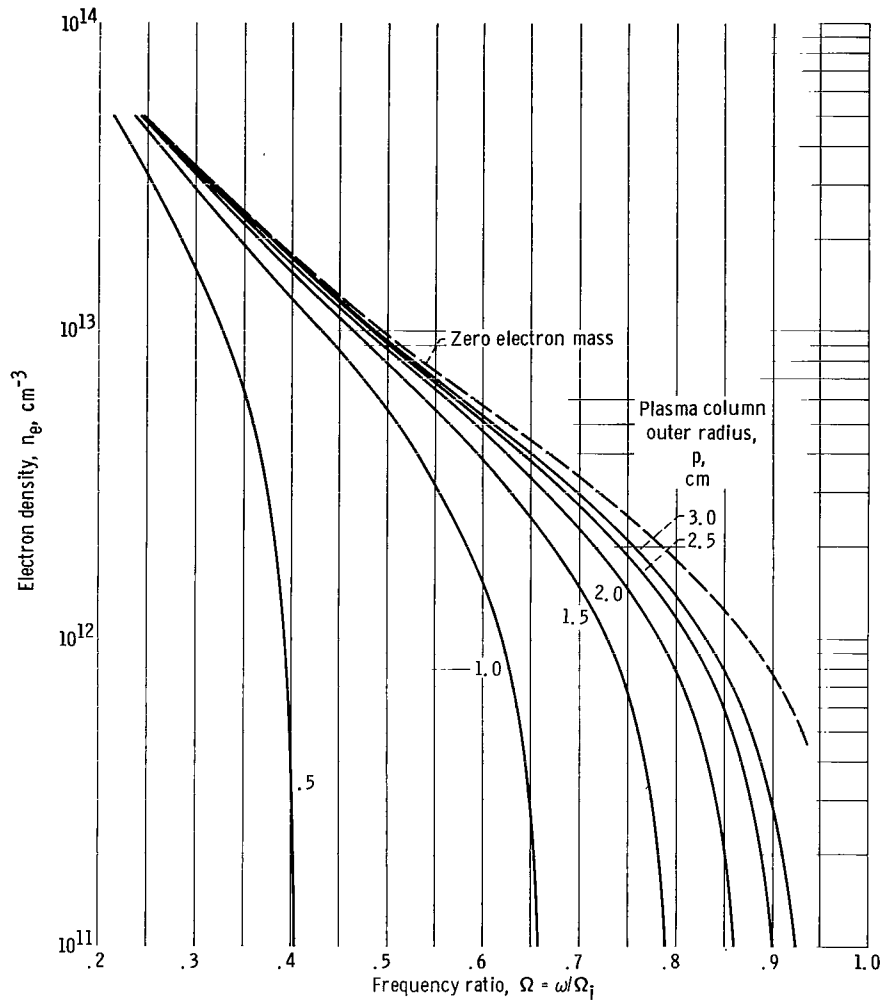


Figure 7. - Frequency ratio as function of electron density for the natural mode with $n = 1$.



(c) Plasma wavelength, 80 centimeters.

Figure 7. - Concluded.

for the natural modes of a plasma column surrounded by a vacuum.

The computer calculations of P_t showed that, for some values of p , n_e , and Ω , only the $n = 1$ mode makes a significant contribution to power transfer. However, for other values of p , n_e , and Ω , and especially for large values of p , several modes make a contribution. When several modes are excited in the plasma at one time, it may be difficult for the experimentalist to make fundamental wavelength measurements to verify the existence of ion cyclotron waves.

Variable Density and Annular Plasmas

The solution for the variable-density cases required a greatly increased amount of

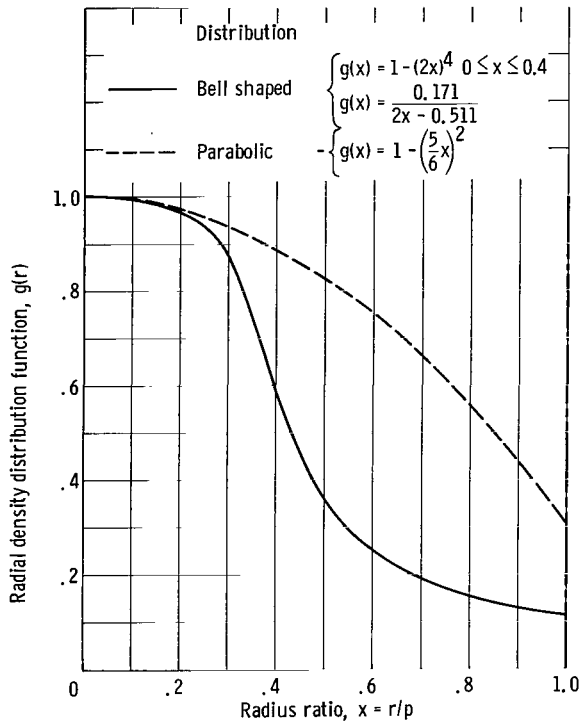


Figure 8. - Radial density distribution as function of radius ratio.

computer time; consequently, a more limited range of plasma parameters was studied. However, enough calculations were made to show the effects of radial density distributions. Figure 8 shows two density-distribution functions that were chosen to illustrate the effects of variable density: the bell-shaped and the parabolic. In addition annular plasmas of constant density whose inner radius, ℓ , was one-half the outer radius, p , were studied. Distributions similar to all three of these have been observed in ion cyclotron wave experiments to date.

Table III gives P_t at maximum for a plasma radius p of 5.0 centimeters, a current-sheet radius s of 10.0 centimeters, and a current I of 92 amperes ($I_{\text{rms}} = 65 \text{ A}$) for several peak density values. The results are for the three density distributions and for constant density. Results for constant density from reference 2, where m_e was assumed to be zero, are also presented in table III.

The effects of including electron inertia

TABLE III. - POWER TRANSFER AT MAXIMUM AS FUNCTION OF PEAK DENSITY FOR SEVERAL DENSITY DISTRIBUTIONS

[Plasma radius, 5.0 cm; current-sheet radius, 10.0 cm; current-sheet wavelength, 45 cm; current, 92 A.]

Peak density, n_0 , cm^{-3}	Density distribution				
	Constant, $m_e = 0$	Constant, $m_e \neq 0$	Bell shaped, $m_e \neq 0$	Parabolic, $m_e \neq 0$	Annular, $m_e \neq 0$, $\ell = 2.5 \text{ cm}$
Power transfer, P_t , kW					
5×10^{10}	58.4	8.2	----	----	----
5×10^{11}	57.8	26.6	16.8	23.2	21.8
5×10^{12}	42.4	34.6	33.6	34.6	31.6
5×10^{13}	13.0	12.4	23.8	11.4	17.8

terms may be seen by examining table III at high densities ($n_e = 5 \times 10^3 \text{ cm}^{-3}$) where the dispersion relations (eqs. (31) and (33)) are essentially identical. Here zero electron mass and finite mass give essentially the same value for $P_{t, \max}$ for constant density. At lower densities, however, the zero-mass results are too high (by an order of magnitude or more for $n_e < 10^{10} \text{ cm}^{-3}$).

For the coil configuration of figure 2(a) (p. 18), there are two current branches. If the current I in each branch is 92 amperes, as was assumed for the calculations in table III, the total current is 184 amperes. Swett (ref. 3) measured the total resistance of a coil of this type and found it to be about 0.3 ohm. Thus, the ohmic loss for 92 amperes is approximately 5 kilowatts. This analysis would then predict that power-transfer efficiencies for the best cases ($m_e \neq 0$) in table III could be as high as 87 percent.

In table III, the use of peak density as a parameter for comparing the different radial density distributions was arbitrary. A more significant parameter might be the volume average density given by

$$\bar{n}_e = \frac{2\pi n_o}{\pi p^2} \int_0^p g(r) r dr$$

where n_o is the maximum density in the plasma. For the bell-shaped distribution, $\bar{n}_e = 0.312 n_o$; for the parabolic distribution, $\bar{n}_e = 0.653 n_o$; and for the annular distribution, $\bar{n}_e = 0.750 n_o$.

In figure 9 P_{\max}^* is shown as a function of this volume average density for the constant-density case and for the three variable-density distributions. The points for the variable-density plasma are in good agreement with the curve for constant density when plotted in this manner. As expected from the strong dependence on plasma radius,

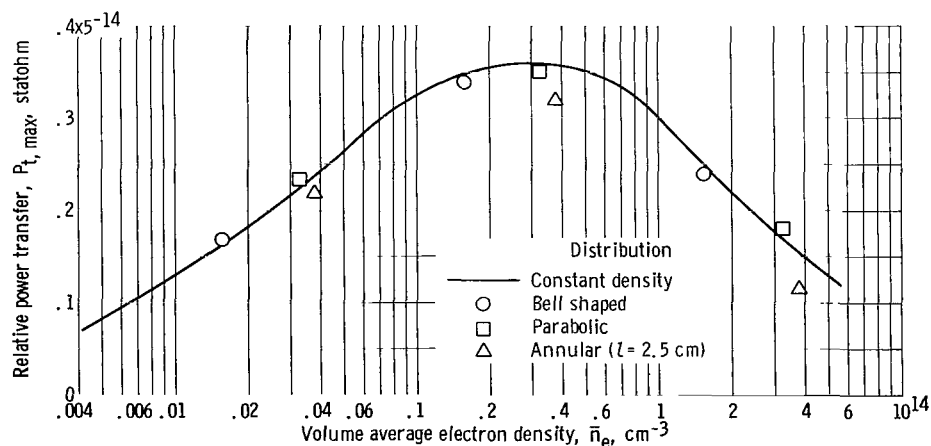


Figure 9. - Relative power transfer as function of volume average electron density.

power transfer to the hollow plasma is almost as great as that to a constant-density plasma with the same outer radius and the same peak density. Apparently, the plasma nearest to the coil carries most of the wave energy.

The importance of the low-density plasma in the tail of the bell-shaped distribution is seen by comparing $P_{t, \max}$ for this distribution with that for the parabolic distribution (in table III) for the same peak density. When the peak density is too high, ($n_0 = 5 \times 10^{13} \text{ cm}^{-3}$) the bell shape is better; but when the peak density is too low ($n_0 = 5 \times 10^{11} \text{ cm}^{-3}$), the parabolic shape is better. When the peak density is about optimum with respect to relative power transfer, $P_{t, \max}$ is the same for the two distributions. The $P_{t, \max}$ for a constant density plasma whose radius is 2.5 centimeters (instead of the 5.0 cm assumed in fig. 9) is less than that of the bell-shaped distribution at all peak densities. Thus, the tail of the bell-shaped distribution is important at all peak densities, but more so at high densities.

The shapes of the curves of P_t as a function of Ω were the same for variable density as those for constant density if the peaks occurred at the same value of Ω in both cases. The widths of the curves are only slightly dependent on the number of modes for which there is significant power input; thus, the widths of the absorption maximums depend primarily on the value of Ω at which peak power transfer occurs.

Different Plasma Modes

Each term in the sum in equation (19b) is regarded as the amount of power put into one of the natural modes of the plasma wave. If the plasma radius is small ($< 5.0 \text{ cm}$) and the density low ($< 10^{12} \text{ cm}^{-3}$), the values of k for the natural modes are widely spaced; so that if $k_1 = k_0$, the majority of the power goes into the first mode because the shape factor $S_r(\eta_n)$ (fig. 5, p. 21) is small for all k_n 's with $n > 1$. When the plasma radius is large and the density is high, the k_n 's are closely grouped, and there can be significant contributions to power for several modes.

It might be expected that, at small plasma radius and low density (where k_n 's are widely spaced), a curve of P_t as a function of Ω might show a maximum each time the k for one of the modes equaled k_0 . This would be true if R_n were the same order of magnitude for several modes. However, the calculations showed that R_n increases or decreases with n in such a way that only a single significant peak results. This single significant peak was found for all constant-density calculations as well as for the variable-density calculations. Thus, if this is the only manner in which power is transferred to the plasma, an experimentalist should see only a single resonance peak in P_t as he varies the magnetic field. Of interest with respect to the results is that for large plasma radii and high density, R_n is a complicated function of Ω with many maximums and min-

imums. Because of the complexity in R_n , the modes that absorb most of the power are continually changing as the magnetic field is varied. For some instances, it was necessary to calculate contributions from as many as 20 modes to determine the total power absorbed by the plasma. When the power is distributed among many modes, the structure of the radial variation of the electric and magnetic fields can be quite complicated.

Effect of Temperature and Collisions

Since one of the reasons for the interest in the production of ion cyclotron waves is their potential for heating the ions of a plasma, a cold plasma model may seem inappropriate. Even when the heating is supposedly localized at a magnetic beach removed from the wave-driving portion, some wave damping may occur throughout the plasma. The applicability of cold plasma results to a hot, collisionless plasma must, therefore, be examined. Stix showed that the dispersion relation for a hot, collisionless plasma reduces to that of a cold plasma when

$$\frac{m_i(\omega - \Omega_i)^2}{2\kappa T_i k^2} \gg 1$$

For a plasma with density $n_e = 5 \times 10^{11}$ per cubic centimeter, peak power transfer occurs at $\Omega \approx 0.95$ and

$$\frac{m_i(\omega - \Omega_i)^2}{2\kappa T_i k^2} = \frac{m_i \Omega_i^2 (1 - \Omega)^2}{2\kappa T_i k^2} \approx \frac{100}{T_i(\text{electron volts})}$$

Thus, for $T_i < 10$ electron volts, the cold-plasma dispersion relation is good at low densities, $n_e = 5 \times 10^{11}$ per cubic centimeter. At higher densities, $1 - \Omega$ is larger at resonance, and the cold-plasma dispersion relation may be used at even higher temperatures.

Under certain conditions, a low-density plasma with a neutral background gas or a high-density plasma may become collision dominated. The following expressions for ion-electron and ion-neutral momentum transfer collision frequencies are given in references 4 and 5, respectively:

$$\nu_{ie} = \frac{m_e}{m_i} \frac{4}{3} \sqrt{\frac{2\pi}{m_e}} \frac{n_e e^4}{(kT_e)^{3/2}} \ln \left[\frac{3}{2\sqrt{\pi}} \frac{(kT)^{3/2}}{e^3 n_e^{1/2}} \right]$$

$$\nu_{in} = 1 \times 10^5 p'$$

where p' is the neutral gas pressure in microns. For an electron temperature of 1 electron volt, $n_e = 5 \times 10^{12}$ per cubic centimeter, and $p' = 2$ microns, the ion-electron collision frequency is

$$\nu_{ie} = 8 \times 10^4 \text{ sec}^{-1}$$

the ion-neutral collision frequency is

$$\nu_{in} = 2 \times 10^5 \text{ sec}^{-1}$$

and the ion collision frequency is

$$\nu_i = \nu_{ie} + \nu_{in} = 2.8 \times 10^5 \text{ sec}^{-1}$$

For an electron temperature of 10 electron volts, ν_{ie} is even less than 8×10^4 per second.

It is probably sufficient to say that the plasma is collisionless when $\nu_i \ll \omega/2\pi$ so that each ion makes many orbits between collisions. The value chosen for $\omega/2\pi$ for the calculations in this report was 6.5×10^6 per second. Since many other ion cyclotron wave experiments in the future may be run at even higher frequencies, the plasma does not become collision dominated unless the density is high and electron-ion collisions predominate. In fact, at the densities of 5×10^{12} per cubic centimeter obtained in this study for optimum power transfer (see tables I and II), the plasma may be considered collisionless.

Wave Reflections

The calculations in this report were made by assuming the presence of an infinitely long plasma column immersed in a uniform magnetic field. Actual laboratory plasmas, however, do not satisfy this assumption, in that, at some distance from the wave-generating current sheets, there may be magnetic mirrors, magnetic beaches (regions where $\Omega \approx 1$), conducting or nonconducting end walls on the plasma test section, and/or other nonuniformities. It is more than likely that some of these nonuniformities will be the cause of wave reflections from the region of nonuniformity back in the direction of the generating structure. If the ion cyclotron wave is sufficiently damped in these regions, the reflected wave is small and its effect on power transfer is negligible. However, a

large reflected wave will pass back under the wave-generating current sheet and may cause constructive or destructive interference there, thus altering the power transfer. To compare this theory with experiment, reflections should be eliminated. It is expected that the most serious wave reflections come from magnetic beach regions, where for low ion temperatures the index of refraction $k_n c/\omega$ changes most rapidly for only small changes in magnetic field. To study these reflections, it is necessary to take into account the effects of nonuniform magnetic fields; near $\Omega = 1$, hot plasma theory must be used.

CONCLUSIONS

Calculations of the power transferred to ion cyclotron waves in both homogeneous and inhomogeneous plasmas by a Stix coil have been made. These calculations show that, for a fixed current-sheet geometry and a constant-density plasma, the power transfer is roughly proportional to the 4.5 power of the plasma radius. For equal plasma current-sheet surface and column outer radii, the power varies as the 3.5 power of plasma radius (or coil radius). If the total current in the current sheet is assumed constant, there is an optimum wavelength that depends on plasma density and radius. The optimum volume average electron density for power transfer is about 5×10^{12} per cubic centimeter.

For electron densities less than 10^{12} per cubic centimeter and for plasma radii less than 5.0 centimeters, most of the power is absorbed by the lowest natural radial mode of the plasma. For electron densities greater than 10^{13} per cubic centimeter and for plasma radii greater than 7.5 centimeter, the power is distributed between several natural modes with the lowest mode not necessarily absorbing the most power. For all cases in which calculations were made, a plot of power transfer as a function of magnetic field gave only one significant resonance peak, regardless of how many modes were absorbing a significant amount of power.

Comparison of the calculations of this report with those of a previous report (NASA TN D-3361), in which a zero-electron-mass dispersion law was used, shows that the zero-electron-mass assumption is valid for a particular mode when the plasma electron density is high. For an electron density less than 5×10^{12} per cubic centimeter, the zero-electron-mass calculations give significantly greater power transfer than that calculated in this report.

Calculations for four different radial density profiles show that power transfer to inhomogeneous plasma columns is high when the volume average density of the plasma is near that density for which power transfer is optimum for constant-density plasmas.

Finally, the applicability of the results presented in this report depends on the degree to which a laboratory plasma is represented by the model used herein.

Lewis Research Center,
National Aeronautics and Space Administration,
Cleveland, Ohio, December 2, 1966,
129-01-05-09-22.

APPENDIX A

SYMBOLS

a	one-half current-sheet length
B	$\frac{k^2(P + S)}{S} - \frac{\omega^2}{c^2} P + \frac{\omega^2}{c^2} \frac{(D^2 - S^2)}{S}$
<u>B</u>	magnetic field vector (time-varying part)
<u>B</u> (r)	radial dependence of <u>B</u>
B ₀	magnitude of <u>B</u> ₀
<u>B</u> ₀	superimposed static magnetic field parallel to z-axis
B _r ^{plasma(vac)}	radial component of <u>B</u> in plasma (vacuum)
B _z ^{plasma(vac)}	axial component of <u>B</u> in plasma (vacuum)
B _θ ^{plasma(vac)}	azimuthal component of <u>B</u> in plasma (vacuum)
C	$\frac{P}{S} \left[k^4 - 2 \frac{\omega^2}{c^2} k^2 S + \frac{\omega^4}{c^4} (S^2 - D^2) \right]$
c	velocity of light
D	D'
D'	eq. (5g)
D ₀	D at peak density
<u>E</u>	electric field vector
E _r ^{plasma(vac)}	radial component of <u>E</u> in plasma (vacuum)
E _z ^{plasma(vac)}	axial component of <u>E</u> in plasma (vacuum)
E _θ ^{plasma(vac)}	azimuthal component of <u>E</u> in plasma (vacuum)
$\left(\mathbf{E}_\theta \right)_{r=s}$	azimuthal component of finite-coil electric field
e	electronic charge
F(k _n s)	radiofrequency-coil-radius correction factor
g(r)	radial density distribution function
I	peak radiofrequency current in current sheet

I_0	modified Bessel function of first kind (zero order)
I_1	modified Bessel function of first kind (first order)
J_0	Bessel function of first kind (zero order)
J_1	Bessel function of first kind (first order)
j^*	magnitude of \underline{j}^*
\underline{j}^*	surface current density vector
$\underline{j}(r)$	plasma current density vector
$\underline{\underline{K}}$	plasma dielectric tensor
$\underline{\underline{K}}'$	$\underline{\underline{K}} - \underline{\underline{1}}$
K_0	modified Bessel function of second kind (zero order)
K_1	modified Bessel function of second kind (first order)
k	plasma wave number
k_n	wave number for n^{th} plasma mode
k_0	current-sheet wave number
L	$L' + 1$
L'	eq. (5d)
\mathcal{L}	linear differential operator, $\frac{\partial}{\partial r} \left(\frac{1}{r} \frac{\partial}{\partial r} r \right)$
ℓ	plasma column inner radius
M	fraction of wavelength covered by one section of Stix coil (see fig. 2)
$\underline{\underline{M}}$	tensor, $\Gamma(k) = \det \underline{\underline{M}}$ for annular plasma column
$\overline{\underline{M}}_{ij}$	elements of $\underline{\underline{M}}$
m_e	electron mass
m_i	hydrogen ion mass (proton mass)
N	number of turns in one section of Stix coil
$n(r)$	electron (ion) density
n_e	electron density
\overline{n}_e	volume average electron density
n_i	ion density
n_0	peak electron density

P	$P' + 1$
P_0	P at peak density
P_t	power transfer (see eq. (19a))
P'	eq. (5e)
P^*	relative power transfer, $P_t/2\pi a^2 j^{*2}$
P^*_{\max}	maximum value of P^* on plot of P^* against Ω
p	plasma column outer radius
p'	background neutral gas pressure
R	$R' + 1$
R'	eq. (5c)
R_n	eq. (17b)
R'_n	eq. (19e)
r	radial cylindrical coordinate
S	$S' + 1$
S'	eq. (5f)
S_0	S at peak density
$S_r(\eta_n)$	shape factor (see eq. (19c))
s	surface current-sheet radius
T_e	electron temperature
T_i	ion temperature
t	time
$\underline{v}_e(r)$	electron vector velocity
$\underline{v}_i(r)$	ion vector velocity
Y_0	Bessel function of second kind (zero order)
Y_1	Bessel function of second kind (first order)
z	axial cylindrical coordinate
α	$\left[S(k^2 + \nu_1^2) - RL \frac{\omega^2}{c^2} \right] / kD$
β	$\left[S(k^2 + \nu_2^2) - RL \frac{\omega^2}{c^2} \right] / kD$

$\Gamma_{1,2,3}(k)$	denominator of eqs. (20), (22), or (26)
γ	$\frac{1}{kp} \frac{K_1(kp)}{K_0(kp)}$
Δ	boundary condition (see eq. (25))
η_n	$2(k_0 - k_n)a$ (eq. (19d))
θ	azimuthal cylindrical coordinate
$\hat{\theta}$	azimuthal unit vector
κ	Boltzmann constant
λ_n	wavelength of n^{th} plasma mode
λ_0	wavelength of surface current sheet
ν_i	ion collision frequency
ν_{ie}	ion-electron collision frequency
ν_{in}	ion-neutral collision frequency
ν_1^2	$\frac{-B + \sqrt{B^2 - 4C}}{2}$
ν_2^2	$\frac{-B - \sqrt{B^2 - 4C}}{2}$
Π_e	electron plasma frequency, $(4\pi n_e e^2 / m_e)^{1/2}$
Π_i	ion plasma frequency, $(4\pi n_i e^2 / m_i)^{1/2}$
Ω	ω / Ω_i
Ω_e	electron cyclotron frequency, $eB_0 / m_e c$
Ω_i	ion cyclotron frequency, $eB_0 / m_i c$
ω	angular frequency of plasma wave
$\underline{\underline{1}}$	unit matrix

APPENDIX B

FUNCTIONS $\Gamma(k)$ AND MATRIX M

The functions $\Gamma_1(k)$ (eq. (20)) and the matrix M used for computing $\Gamma_2(k)$ are given as follows:

For the solid cylinder ($\ell = 0$):

$$\begin{aligned} \Gamma_1(k) = \alpha & \left[P J_1(\nu_1 p) + \gamma \nu_1 p J_0(\nu_1 p) \right] \left[\gamma \nu_2 p J_0(\nu_2 p) + J_1(\nu_2 p) \right] \\ & - \beta \left[P J_1(\nu_2 p) + \gamma \nu_2 p J_0(\nu_2 p) \right] \left[\gamma \nu_1 p J_0(\nu_1 p) + J_1(\nu_1 p) \right] \end{aligned}$$

For the annular cylinder ($\ell \neq 0$):

$$M = (M_{ij}) \quad i, j = 1, 2, 3, 4$$

$$\Gamma_2 = \det M$$

$$M_{11} = \alpha \left[J_1(\nu_1 \ell) - \frac{\nu_1 J_0(\nu_1 \ell) I_1(k \ell)}{P k I_0(k \ell)} \right]$$

$$M_{12} = \beta \left[J_1(\nu_2 \ell) - \frac{\nu_2 J_0(\nu_2 \ell) I_1(k \ell)}{P k I_0(k \ell)} \right]$$

$$M_{13} = \alpha \left[Y_1(\nu_1 \ell) - \frac{\nu_1 Y_0(\nu_1 \ell) I_1(k \ell)}{P k I_0(k \ell)} \right]$$

$$M_{14} = \beta \left[Y_1(\nu_2 \ell) - \frac{\nu_2 Y_0(\nu_2 \ell) I_1(k \ell)}{P k I_0(k \ell)} \right]$$

$$M_{21} = J_1(\nu_1 \ell) - \frac{\nu_1 J_0(\nu_1 \ell) I_1(k \ell)}{k I_0(k \ell)}$$

$$M_{22} = J_1(\nu_2 \ell) - \frac{\nu_2 J_0(\nu_2 \ell) I_1(k \ell)}{k I_0(k \ell)}$$

$$M_{23} = Y_1(\nu_1 \ell) - \frac{\nu_1 Y_0(\nu_1 \ell) I_0(k \ell)}{k I_0(k \ell)}$$

$$M_{24} = Y_1(\nu_2 \ell) - \frac{\nu_2 Y_0(\nu_2 \ell) I_1(k \ell)}{k I_0(k \ell)}$$

$$M_{31} = \alpha \left[J_1(\nu_1 p) + \frac{\nu_1 J_0(\nu_1 p) K_1(k p)}{p k K_0(k p)} \right]$$

$$M_{32} = \beta \left[J_1(\nu_2 p) + \frac{\nu_2 J_0(\nu_2 p) K_1(k p)}{p k K_0(k p)} \right]$$

$$M_{33} = \alpha \left[Y_1(\nu_1 p) + \frac{\nu_1 Y_0(\nu_1 p) K_1(k p)}{p k K_0(k p)} \right]$$

$$M_{34} = \beta \left[Y_1(\nu_2 p) + \frac{\nu_2 Y_0(\nu_2 p) K_1(k p)}{p k K_0(k p)} \right]$$

$$M_{41} = J_1(\nu_1 p) + \frac{\nu_1 J_0(\nu_1 p) K_1(k p)}{k K_0(k p)}$$

$$M_{42} = J_1(\nu_2 p) + \frac{\nu_2 J_0(\nu_2 p) K_1(k p)}{k K_0(k p)}$$

$$M_{43} = Y_1(\nu_1 p) + \frac{\nu_1 Y_0(\nu_1 p) K_1(k p)}{k K_0(k p)}$$

$$M_{44} = Y_1(\nu_2 p) + \frac{\nu_2 Y_0(\nu_2 p) K_1(k p)}{k K_0(k p)}$$

In the preceding expressions for Γ_1 and M_{ij} , ν_1^2 and ν_2^2 were assumed to be positive. When ν_1^2 or ν_2^2 is negative, $\nu_{1,2}$ is replaced by $\sqrt{|\nu_{1,2}^2|}$, $J_0(x)$ by $I_0(x)$, $J_1(x)$ by $I_1(x)$, $Y_0(x)$ by $-K_0(x)$ and $Y_1(x)$ by $K_1(x)$, where $x = \sqrt{|\nu_{1,2}^2|} \cdot y$, and y is either p or l . However, α and β are not changed.

APPENDIX C

SOLVING FOR NATURAL MODES

For the constant-density plasma where the electric fields of an infinitely long plasma column are known analytic functions of k , the condition $\Gamma = 0$ for natural modes results in one equation with k as the only variable. Then, k is varied until this equation is satisfied.

For the inhomogeneous plasma, the boundary conditions can be combined so that there are two conditions, $\Gamma = 0$ and $\Delta = 0$, for natural modes, and also two unknowns, k and $\left[\frac{\partial^3 E_\theta(r)}{\partial r^3} \right]_{r=0} = E''''$. Thus,

$$\Gamma = \Gamma_0 + \frac{\partial \Gamma_0}{\partial k} dk + \frac{\partial \Gamma_0}{\partial E''''} dE'''' \quad (C1)$$

$$\Delta = \Delta_0 + \frac{\partial \Delta_0}{\partial k} dk + \frac{\partial \Delta_0}{\partial E''''} dE'''' \quad (C2)$$

where

$$\Gamma = \Gamma(k_b, E_b''') \quad \Gamma_0 = \Gamma(k_a, E_a''')$$

$$\Delta = \Delta(k_b, E_b''') \quad \Delta_0 = \Delta(k_a, E_a''')$$

$$dE'''' = E_b'''' - E_a'''' \quad dk = k_b - k_a$$

The values of Γ_0 and Δ_0 are the values of Γ and Δ for a set of trial values of k and E'''' , to be designated k_a and E_a'''' . Setting $\Gamma = 0$ and $\Delta = 0$ in equations (C1) and (C2) yields two equations and two unknowns, dk and dE'''' that may be determined by Cramer's rule:

$$dk = \frac{\begin{vmatrix} -\Gamma_o & \frac{\partial \Gamma_o}{\partial E'''} \\ -\Delta_o & \frac{\partial \Delta_o}{\partial E'''} \end{vmatrix}}{\begin{vmatrix} \frac{\partial \Gamma_o}{\partial k} & \frac{\partial \Gamma_o}{\partial E'''} \\ \frac{\partial \Delta_o}{\partial k} & \frac{\partial \Delta_o}{\partial E'''} \end{vmatrix}} \quad dE''' = \frac{\begin{vmatrix} \frac{\partial \Gamma_o}{\partial k} & -\Gamma_o \\ \frac{\partial \Delta_o}{\partial k} & -\Delta_o \end{vmatrix}}{\begin{vmatrix} \frac{\partial \Gamma_o}{\partial k} & \frac{\partial \Gamma_o}{\partial E'''} \\ \frac{\partial \Delta_o}{\partial k} & \frac{\partial \Delta_o}{\partial E'''} \end{vmatrix}}$$

The value of k is then changed by dk and the value of E'''_a is changed by dE''' ; and Δ_o and Γ_o are computed again. This Newton-Raphson procedure is repeated until Δ_o and Γ_o converge sufficiently close to zero.

Two problems arise when the previous procedure is used: first, because of the nature of Γ and Δ , it is possible that there will be no convergence at all; second, there may be convergence, but to the wrong mode. These problems can be overcome by plotting Γ as a function of k , under the single constraint $\Delta = 0$ for a single set of the values, Ω and Π_e^2 . The $\Gamma = 0$ points then give the values of k for the natural mode. Since this latter technique takes considerable computer time, the following procedure was adopted:

(1) For a given density distribution $g(r)$, values for Ω and Π_e^2 were chosen and the procedure described in the previous paragraph was followed to find the values of k and E''' for the natural modes.

(2) Trial values of k_a for other values of Ω_a and $\Pi_e^2_a$ were obtained from the cold-plasma zero-electron-mass dispersion law and from the values computed in item (1):

$$\frac{k_a^2}{k^2} = \frac{\left(\Pi_e^2\right)_a \Omega_a^2 (1 - \Omega^2)}{\Pi_e^2 \Omega^2 (1 - \Omega_a^2)}$$

(3) These trial values of k_a obtained in item (2) and E'''_o from item (1) could then be used in the Newton-Raphson method to find natural modes.

REFERENCES

1. Stix, Thomas H. : The Theory of Plasma Waves. McGraw-Hill Book Co. , Inc. , 1962.
2. Sigman, Donald R. : Radiofrequency Power Transfer to Ion-Cyclotron Waves in a Collision-Free Magnetoplasma. NASA TN D-3361, 1966.
3. Swett, Clyde C. : Effect of Magnetic Beach on Radiofrequency Power Absorption in Ion Cyclotron Resonance. Paper presented at the American Physical Society Meeting, Minneapolis, June 20-22, 1966.
4. Longmire, Conrad, L. : Elementary Plasma Physics. Interscience Publ. , Inc. , 1963.
5. Buchsbaum, S. J. : Electron and Ion Resonance in a Plasma. Physics Today, vol. 15, no. 12, Dec. 1962, pp. 32-36.

"The aeronautical and space activities of the United States shall be conducted so as to contribute . . . to the expansion of human knowledge of phenomena in the atmosphere and space. The Administration shall provide for the widest practicable and appropriate dissemination of information concerning its activities and the results thereof."

—NATIONAL AERONAUTICS AND SPACE ACT OF 1958

NASA SCIENTIFIC AND TECHNICAL PUBLICATIONS

TECHNICAL REPORTS: Scientific and technical information considered important, complete, and a lasting contribution to existing knowledge.

TECHNICAL NOTES: Information less broad in scope but nevertheless of importance as a contribution to existing knowledge.

TECHNICAL MEMORANDUMS: Information receiving limited distribution because of preliminary data, security classification, or other reasons.

CONTRACTOR REPORTS: Scientific and technical information generated under a NASA contract or grant and considered an important contribution to existing knowledge.

TECHNICAL TRANSLATIONS: Information published in a foreign language considered to merit NASA distribution in English.

SPECIAL PUBLICATIONS: Information derived from or of value to NASA activities. Publications include conference proceedings, monographs, data compilations, handbooks, sourcebooks, and special bibliographies.

TECHNOLOGY UTILIZATION PUBLICATIONS: Information on technology used by NASA that may be of particular interest in commercial and other non-aerospace applications. Publications include Tech Briefs, Technology Utilization Reports and Notes, and Technology Surveys.

Details on the availability of these publications may be obtained from:

SCIENTIFIC AND TECHNICAL INFORMATION DIVISION
NATIONAL AERONAUTICS AND SPACE ADMINISTRATION
Washington, D.C. 20546